Original Article
Microenvironment of mammary fat pads affected the characteristics of the tumors derived from the induced cancer stem cells

Hagar A Abu Quora[1,2*], Maram H Zahra[1*], Samah El-Ghlban[3], Neha Nair[4], Said M Afify[1,3], Ghmkin Hassan[1], Hend M Nawara[1], Mona Sheta[1], Sadia Monzur[1], Xiaoying Fu[1,5], Amira Osman[6], Akimasa Seno[1], Masaharu Seno[1]

[1]Department of Biotechnology and Drug Discovery, Graduate School of Interdisciplinary Science and Engineering in Health Systems, Okayama University, Okayama 700-8530, Japan; [2]Cytology, Histology and Histochemistry, Zoology Department, Faculty of Science, Menoufia University, Menoufia 32511, Egypt; [3]Division of Biochemistry, Faculty of Science, Menoufia University, Menoufia 32511, Egypt; [4]Department of Medical Bioengineering, Graduate School of Natural Science and Technology, Okayama University, Okayama 700-8530, Japan; [5]Department of Pathology, Tianjin University of Traditional Chinese Medicine, Tianjin 300193, China; [6]Department of Histology, Faculty of Medicine, Kafr Elsheikh University, Kafr Elsheikh 33511, Egypt. *Equal contributors.

Abstract: Breast cancer is the first common cause of cancer-related death in women worldwide. Since the malignancy and aggressiveness of breast cancer have been correlated with the presence of breast cancer stem cells, the establishment of a disease model with cancer stem cells is required for the development of a novel therapeutic strategy. Here, we aimed to evaluate the availability of cancer stem cell models developed from mouse induced pluripotent stem cells with the conditioned medium of different subtypes of breast cancer cell lines, the hormonal-responsive T47D cell line and the triple-negative breast cancer BT549 cell line, to generate in vivo tumor models. When transplanted into the mammary fat pads of BALB/c nude mice, these two model cells formed malignant tumors exhibiting pronounced histopathological characteristics similar to breast cancers. Serial transplantation of the primary cultured cells into mammary fat pads evoked the same features of breast cancer, while this result was perturbed following subcutaneous transplantation. The tumors formed in the mammary fat pads exhibited immune reactivities to prolactin receptor, progesterone receptor, green florescent protein, Ki67, CD44, estrogen receptor α/β and cytokeratin 8, while all of the tumors and their derived primary cells exhibited immunoreactivity to estrogen receptor α/β and cytokeratin 8. Cancer stem cells can be developed from pluripotent stem cells via the secretory factors of cancer-derived cells with the capacity to inherit tissue specificity. However, cancer stem cells should be plastic enough to be affected by the microenvironment of specific tissues. In summary, we successfully established a breast cancer tumor model using mouse induced pluripotent stem cells developed from normal fibroblasts without genetic manipulation.

Keywords: Mammary fat pad, microenvironment, iPSCs, CSCs, breast cancer

Introduction

Cancer is the most serious disease in the world, and the rate of incidence of new cases is still high. Breast cancer (BC) is the first common cause of cancer-related death in women worldwide. The crude rates per 100,000 population of BC occurrence in 2020 are estimated to be 45 in Asia, 137 in Europe, 151 in North America, and 28 in Africa according to WHO 2020. BC represents approximately 25% of all types of cancer [1]. BC is characterized by distinct stages, from atypical ductal hyperplasia (ADH) and ductal carcinoma in situ (DCIS) to invasive breast cancer [2]. Several studies have reported that the cause of tumors, including BC, is attributed to the presence of small numbers of heterogeneous cell populations. These small cell populations are called cancer stem cells (CSCs), which represent approximately 1 to 5%

of all cells in tumor tissue [3]. CSCs are characterized by their potential for self-renewal, differentiation and tumorigenesis [4, 5], resulting in increasing rates of tumor progression [6], cell mobility [7, 8], cell invasion and metastasis [9, 10] together with the formation of blood vessels for angiogenesis. Recently, the role of CSCs in BC has been clarified by the expression of some cell surface markers on cells isolated from tumors [3]. However, the analyses of CSCs in tumor tissues have not been efficient and practical due to their low abundance.

Previously, our group successfully developed unique models of CSCs from induced pluripotent stem cells (iPSCs), which were developed from normal embryonic fibroblasts, in the presence of conditioned medium (CM) from a cancer cell culture mimicking the tumor microenvironment [11]. Using this model, we found that CSCs may generate cancer-associated cells, such as vascular endothelial cells, cancer-associated fibroblasts (CAFs) [12], tumor-associated adipocytes and tumor-associated macrophages (TAMs) [13], which form a part of the tumor microenvironment (TME) [14]. Thus, CSCs appear to be supported and maintained in heterogeneous tumor tissues, creating a niche that maintains the balance between self-renewal and differentiation [15]. During the course of the studies, we successfully established two different tissue-specific models, a pancreatic ductal adenocarcinoma CSC model [16] and a liver CSC model [17], both of which were converted from mouse iPSCs (miPSCs) in the presence of CM from pancreatic cancer cells and liver cancer cells, respectively, developed via the effects of tissue-specific factors *in vivo.* In conclusion, the TME can be considered a mixture of microenvironments that are generated by CSCs on the one hand and by adjacent normal tissues on the other hand.

In the present study, we aimed to establish an *in vivo* breast cancer model of CSCs converted from miPSCs with CM from different subtypes of BC cell lines via transplantation by comparing the phenotypes that may be plastic depending on the microenvironment, such as the mammary fat pad (MFP) and subcutaneous (s.c.) tissue.

Materials and methods

Cell cultures

The CSC models miPS-T47Dcm and miPS-BT549cm cells, were previously prepared by our group [12]. The human breast cancer cell line T47D, which was derived from the pleural effusion of a ductal carcinoma found in the mammary gland of an elderly human patient, and the cell line BT549, which was derived from triple-negative breast cancer, were obtained from Riken Cell Bank, Japan. The normal mouse mammary epithelial cell line NMuMG was a kind gift from Dr. David Salomon under an MTA of the National Cancer Institute, MD. The cells were cultured in RPMI-1640 medium (WAKO, Japan) supplemented with 10% fetal bovine serum (FBS) (Gibco®, Life Technologies™, USA) and 100 U/ml penicillin/streptomycin (P/S) (Nacalai Tesque, Japan). The cells were cultured and maintained in a 37°C incubator with 5% CO_2 until reaching 80% confluence. To prepare the CM, the medium was supplemented with 5% FBS, and after 48 h, the medium was collected, centrifuged for 10 min at 1000 rpm and then filtered through a 0.22 µm filter (Millipore, Ireland). The CM was stored at -20°C until use. The miPSCs (iPS MEF-Ng-20D-17, Riken Cell Bank, Japan) [18] were maintained in DMEM supplemented with 15% FBS, 0.1 mM MEM with nonessential amino acids (Wako, Japan), 2 mM L-glutamine, 100 U/ml P/S (Nacalai Tesque, Japan), 0.1 mM 2-mercaptoethanol (Sigma-Aldrich, USA), and 1000 U/ml leukemia inhibitory factor (WAKO, Japan) on a feeder layer of mitomycin-treated mouse embryonic fibroblast (MEF) cells (Reprocell, Japan) seeded at $5×10^4$ cells in a 60-mm dish (TPP, Switzerland). The miPSCs were seeded at $5×10^5$ cells on MEFs coated with 0.1% gelatin (Sigma, USA) and maintained under the same conditions.

Animal experiments

Four-week-old female BALB/c-nu/nu mice were purchased from Charles River, Japan. The experimental animals were divided into the s.c. and MFP groups. For transplantation, $1×10^6$ cells were suspended in 100 µl of Hank's balanced salt solution (Gibco®, Life Technologies™, USA) and injected dorsally into the s.c. tissue or into one of the fourth pair (4G) of MFP. The experimental protocol is summarized in **Figure 1A**. In the primary (P) tumors, miPS-T47Dcm and miPS-BT549cm cells were injected into s.c. tissue or MFPs. The tumors obtained from the s.c. group were named Ts.c./Bs.c., while the tumors obtained from the MFP group were named Tm1/Bm1. Mice were sacrificed after

A

B

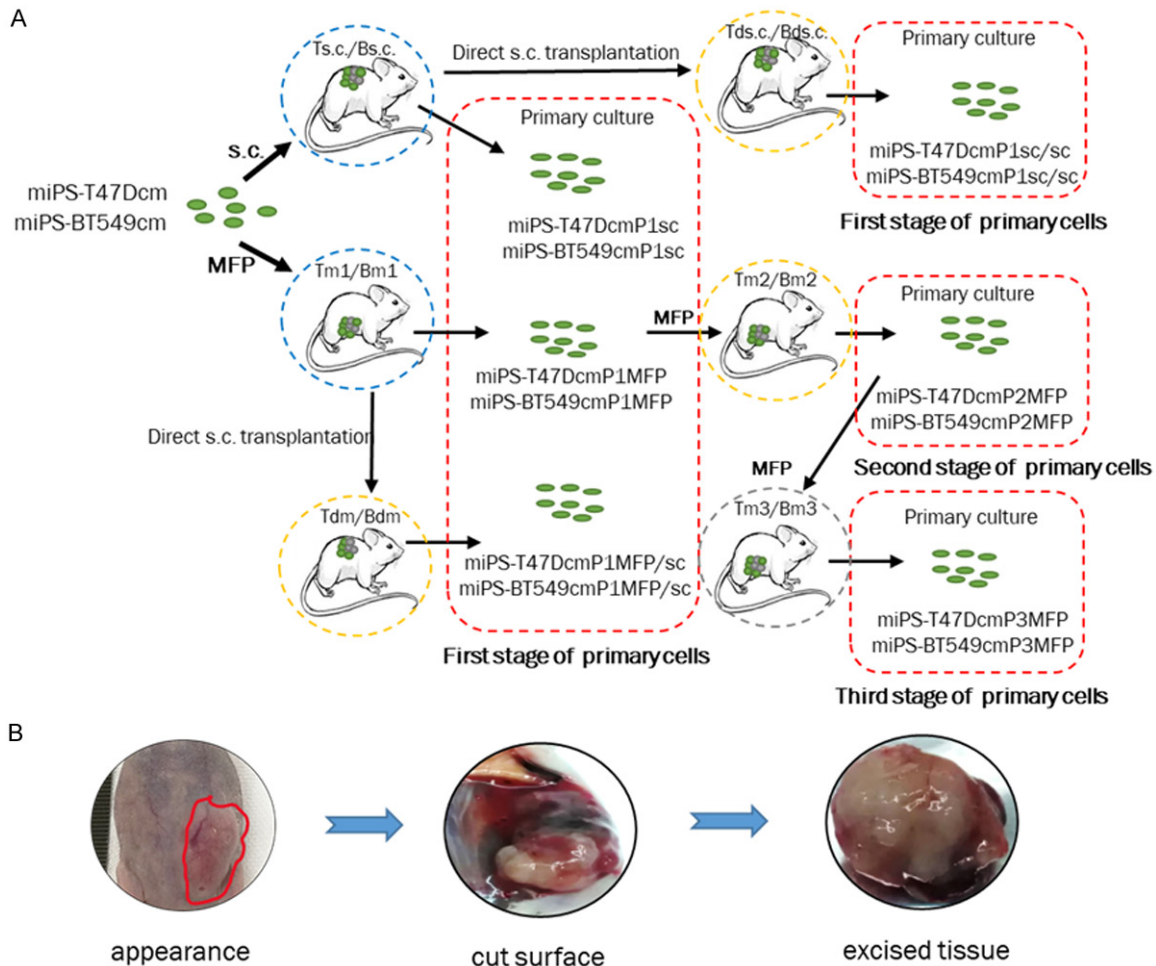appearance   cut surface   excised tissue

Figure 1. A. Schematic drawing of the preparation of primary cells. The first stage: miPS-T47DcmP1sc, miPS-BT549cmP1sc, miPS-T47DcmP1sc/sc, miPS-BT549cmP1sc/sc, miPS-T47DcmP1MFP, miPS-BT549cmP1MFP, miPS-T47DcmP1MFP/sc and miPS-BT549cmP1MFP/sc cells from the tumors developed from the transplantation of miPS-T47Dcm and miPS-BT549cm cells in BALB/c-nu/nu mice. The second stage of primary cells is the P culture of the Tm2/Bm2 tumors. The third stage of primary cells is the P culture of the Tm3/Bm3 tumors. Each stage of primary cells is surrounded by red broken squares. Ts.c./Bs.c. and Tm1/Bm1 are the primary tumors (blue broken circles). Tds.c./Bds.c., Tm2/Bm2 and Tdm/Bdm are the secondary tumors (yellow broken circles). Tm3/Bm3 is the tertiary tumor (gray broken circles). B. The macroscopic features of the Tm1 tumor transplanted into the MFPs. The border of the tumor was ill defined (red line) with a firm consistency that was too hard (left). The cut surface shows hemorrhage and necrotic areas (middle). The base appears indurated and infiltrating (right).

approximately 4 weeks when the size of the tumor reached approximately 1 cm in diameter. Immediately after sacrifice, tissues from Ts.c./Bs.c. and Tm1/Bm1 tumors were directly transplanted into s.c. tissue to obtain tumors named Tds.c./Bds.c. and Tdm/Bdm. P1 cultures from Tm1/Bm1 tumors were prepared as described by Chen et al. (2012), and the obtained cells, named miPS-T47DcmP1MFP and miPS-BT549cmP1MFP, were injected into the MFPs to yield the secondary tumors, named Tm2/Bm2. After 4 weeks, the mice were sacrificed, and P cultures from Tm2/Bm2 tumors

were prepared according to Chen et al. (2012). The obtained cells, miPS-T47DcmP2MFP and miPS-BT549cmP2MFP, were injected into the MFPs to yield tertiary tumors, Tm3/Bm3. The present study was approved by the Animal Care Use Committee of Okayama University under IDs OKU-2020382 and OKU-2020652.

Histopathological analysis

For the histopathological analysis, tumors were immediately removed from mice, fixed in 10% neutral formalin (Wako, Japan) for 24 h, and

embedded in molten paraffin wax (Wako, Japan). Then, the paraffin blocks were cut by using an automatic rotary microtome (HistoCore AUTOCUT, Leica, Germany) with a 5 µm thickness. Then, sections were stained with hematoxylin (Merck, Germany) and counterstained with alcoholic 0.5% Eosin Y (Wako, Japan). Sections were examined by using an Olympus FSX100 microscope (Olympus, Tokyo, Japan), and images were captured with an FSX100 digital camera (Olympus) and processed with FSX-BSW version 3.2. software (Olympus) on 10x NA0.40 and 20x NA0.95 objective lenses.

Immunohistochemical (IHC) analysis

Paraffin sections with a thickness of 5 µm were stained for IHC analysis according to the procedures of the ABC Vectastain kit with an Elite anti-rabbit IgG antibody (Vector Laboratories, USA). Protein expression was detected by using DAB substrates (Vector Laboratories, USA) and counterstained with hematoxylin. The primary antibodies used in this study were as follows: anti-mouse estrogen receptor beta (ERβ) rabbit polyclonal antibody (1:50, ab3576, Abcam, UK), anti-mouse progesterone receptor (PR) rabbit polyclonal antibody (1:100, ab63605, Abcam, UK), anti-mouse prolactin receptor (PRL-R) rabbit monoclonal antibody (1:50, ab170935, Abcam, UK), anti-mouse CD44 rabbit polyclonal antibody (1:200, ab24504, Abcam, UK), anti-mouse Ki67 rabbit polyclonal antibody (1:100, ab66155, Abcam, UK), and anti-mouse green florescent protein (GFP) rabbit monoclonal antibody (1:500, #2956, Cell Signaling Technology, USA). The negative control sections were prepared identically to all other slides, but the primary antibody was replaced with an isotype rabbit IgG (Wako, Japan). Slides were examined, and images were taken as described above on an LCACHN40xPHP NA0.55 objective lens.

Immunofluorescence analysis

For the immunofluorescence analysis, paraffin sections with a 5 µm thickness were dewaxed, rehydrated and treated by antigen retrieval (trisodium citrate dihydrate). The sections were incubated with the following primary antibodies overnight at 4°C: anti-mouse estrogen receptor α (ERα) mouse monoclonal antibody (1:50, sc-8005; Santa Cruz Biotechnology, CA) and anti-mouse cytokeratin 8 (CK8) mouse mono-

clonal antibody (1:50, sc-8020; Santa Cruz Biotechnology, CA). Then, the slides were incubated with Alexa Fluor® 594-labeled goat anti-mouse IgG (1:1000, ab150116; Abcam, UK). Nuclei were counterstained by mounting with antifade mounting medium containing 4,6-diamidino-2-phenylindole (DAPI; Vector laboratories). The negative control sections were prepared identically to all other slides, but the primary antibody was replaced with an isotype mouse IgG (Wako, Japan) (**Figure 12**). Slides were examined, and images were taken by using an Olympus FSX100 microscope (Olympus, Tokyo, Japan) on an LCACHN40xPHP NA0.55 objective lens. The florescence filters used to capture the florescence digital images included a green filter (U-MWIBA3), red filter (U-MWIG3) and blue filter (U-MNUA2).

Immunocytochemical analysis

The cells were seeded at 1×10^5 cells/well in a 12-well plate that contained a gelatin-coated coverslip in each well. The plate was incubated at 37°C with 5% CO_2 until cells were attached. Then, the medium was carefully aspirated, and the wells were washed 3 times with PBS. Then, the cells were fixed with 4% paraformaldehyde (Nacalai Tesque, Japan) for 20 min. The cells were permeabilized with 0.1% Triton X-100 (Nacalai Tesque, Japan) in PBS and blocked in 1% bovine serum albumin (Sigma, USA) followed by several washes with PBS and incubation with the primary anti-mouse ERα rabbit monoclonal antibody (1:1000, ab32063; Abcam, UK) and anti-mouse PR rabbit polyclonal antibody (1:500, ab63605; Abcam, UK) overnight at 4°C. At that time, the cells were washed with PBS and incubated with Alexa Fluor 555®-labeled goat anti-rabbit IgG (H+L) (1:1000, A21428; Invitrogen Thermo Fisher Scientific, USA) for 1 h at room temperature. Then, slides were mounted with antifade mounting medium containing DAPI (Vector Laboratories). Slides were examined, and images were taken as described above.

Protein extraction and western blotting

Total protein of cells or tissues was extracted with lysis buffer (1 M Tris-HCl, pH 8, 5 M NaCl, 10% Triton, 0.4 M EDTA and Mill Q H_2O) containing a proteinase inhibitor cocktail (225955-11, Nacalai Tesque, Japan). The proteins were subjected to 12.5% SDS-PAGE, and then proteins

were transferred to polyvinylidene difluoride membranes (Millipore-Merck, Germany). The membranes were then blocked in 5% skim milk by shaking for 1 h at room temperature, and then the membranes were incubated with the primary anti-mouse β-actin monoclonal antibody (1:1000, 010-27841; Wako, Japan), anti-mouse ERβ rabbit polyclonal antibody (1:1000, ab3576; Abcam, UK), anti-mouse ERα mouse monoclonal antibody (1:200, sc-8005; Santa Cruz Biotechnology, CA) and anti-mouse CK8 mouse monoclonal antibody (1:200, sc-8020; Santa Cruz Biotechnology, CA) overnight at 4°C followed by incubation with horseradish peroxidase-conjugated anti-rabbit/mouse IgG (1:1000, #7074s/#7076s, Cell Signaling Technology, MA) as the secondary antibody for 1 h at room temperature. Immunoreactivity on the membrane was developed, and images were captured by WSE-6100H-ACP LuminoGraph I and processed with ImageSaver6 version 2.7.2 software (ATTO Bioscience and Biotechnology; Tokyo, Japan).

RNA isolation and reverse transcription quantitative PCR (RT-qPCR)

Total RNA of cells or tissues was isolated with TRIzol (Life Technologies, USA) following the manufacturer's protocol. The extracted RNA was treated with DNase I (Promega, Nasison, W.I., USA). One microgram of RNA was reverse transcribed with the GoScript™ Reverse Transcription System (Promega, Nasison, W.I, USA). RT-qPCR was performed with Light Cycler 480 SYBR green I Master Mix (Roche Diagnostics GmbH, Germany) on a Light Cycler 480 II (Roche Diagnostics GmbH, Germany) following the manufacturer's instructions. All primers used in this study were designed with bioinformatics tools, such as BLAST (NCBI, Bethesda, MD, USA) and Primer3 tools (**Table 1**), and synthesized by Eurofins Genomics, Japan.

Image analysis

Digital IHC and Western blotting images were analyzed by a semiquantitative scoring system (Fiji-ImageJ software, Java-based application for analyzing images) (http://imagej.nih.gov/ij/). The percentage of the stained area (area fraction) was determined by measuring six randomly photographed high-power fields 20× [19]. Additionally, this program was applied to compare the density of bands of different immunoreactive proteins on Western blot.

Statistical analysis

All data obtained are expressed as the mean ± standard deviation (mean ± SD). The significance between different groups was evaluated by using one-way ANOVA.

Results

Focusing on the pathological signatures of breast cancer including ERα/β, PR and PRL-R, we investigated the characteristics of Ts.c./Bs.c., Tm1/Bm1, Tds.c./Bds.c., Tdm/Bdm, Tm2/Bm2 and Tm3/Bm3 tumors derived from CSC models of miPS-T47Dcm and miPS-BT549cm cells and their primary cultures in this study (**Figure 1A**).

Macroscopic features of the tumors

The macroscopic features of the developed tumors indicated that these tumors were malignant when transplanted into either the MFPs or s.c. tissue. A representative tumor is shown in **Figure 1B**. The border of the tumor was ill defined with a firm consistency that was not too hard. The cut surface appears with hemorrhage and necrotic areas as well as an indurated and infiltrating base.

Morphological characteristics of the tumors as BC

The tumors showed different histopathological features under microscopic examinations. Those of Ts.c./Bs.c. and Tm1/Bm1 (**Figures 2**, **3**). Pronounced characteristics of histopathological malignancies, such as invasive lobular carcinoma (ILC) like structures with small round nuclei, inconspicuous nuclei and scant cytoplasm, were observed in the Tm1 tumor of miPS-T47Dcm cells that were implanted into the MFPs (**Figure 2A**). Tumors of miPS-T47DcmP1 cells transplanted into the MFPs, which formed Tm2 tumors, resembled ADH, solid DCIS and high mitotic activity with a gastrointestinal structure (**Figure 2B**). In the tertiary Tm3 tumor in which miPS-T47DcmP2 cells were transplanted into the MFPs, duct ectasia with fatty necrosis, adenosis, active mitogenic cells and lymph node metastasis with a focal legion and disrupted capsule like structures were
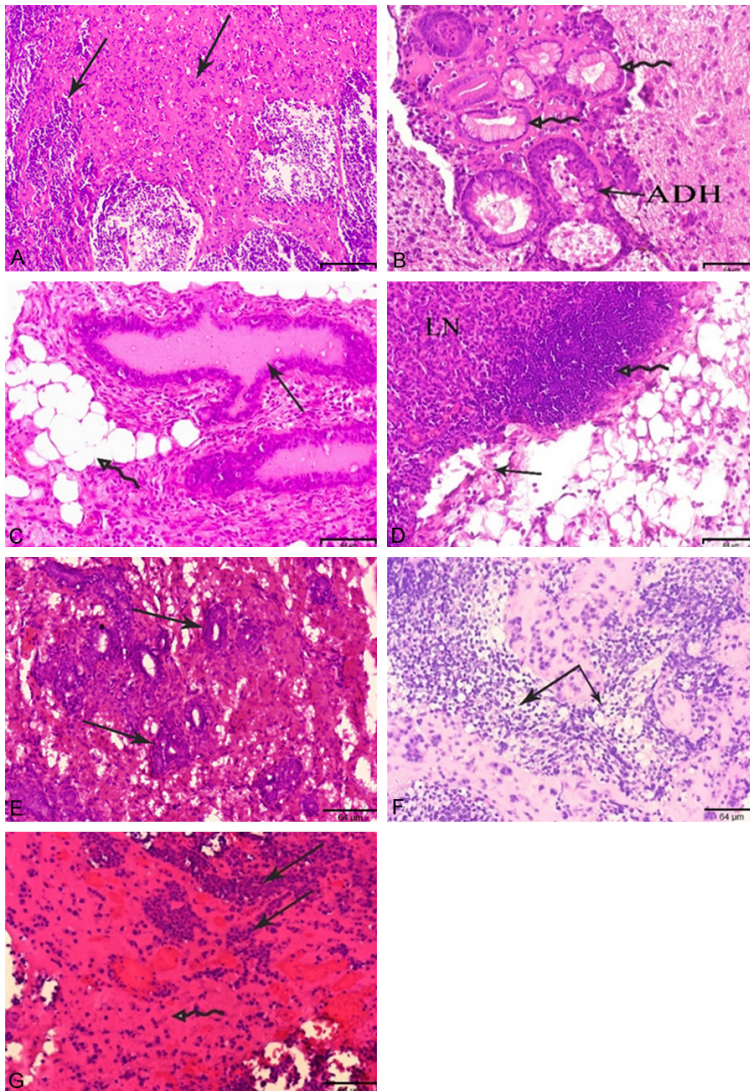
Figure 2. Histopathological observations in the sections of tumors, Tm1, Tm2, Tm3, Ts.c., Tdm and Tds.c. obtained from miPS-T47Dcm cells transplanted in BALB/c-nu/nu mice. (A-D, F) Tumors developed in MFP (E, G) Tumors developed in s.c. Arrows indicate ILC (A) ADH and gastrointestinal structure (B) duct ectasia with fatty necrosis and adenosis (C, lymph node metastasis (LN) with focal legion and disrupted capsule (D) adenosis (E) ILC (F) active mitogenic cells with necrotic areas (G) like structures, Hematoxylin and Eosin, scale bar = 129 μm at 10× magnification, 64 μm at 20× magnification.

genic cells and necrotic areas were recognized in the Tds.c. tumor, which was directly transplanted from a Ts.c. tumor (**Figure 2G**).

In the Bm1 tumor in which miPS-BT549cm cells were transplanted into the MFPs, resembled high-grade DCIS with central comedo necrosis, solid DCIS with a completely filled duct characterized by enlarged pleomorphic nuclei, fibrocystic dilated ducts and adenosis were observed (**Figure 3A**). The similar characteristic of ILC with small nuclei and cytoplasmic vacuolation surrounded by fibers was found in the Bm2 tumor of miPS-BT549cmP1 cells transplanted into the MFPs (**Figure 3B**), while medullary carcinoma with pleomorphic nuclei surrounded by fibers and infiltrated lymphatic cells like structure was detected in the Bm3 tumor of miPS-BT549cmP2 cells transplanted into the MFPs (**Figure 3C**). In the Bs.c. tumor of miPS-BT549cm cells transplanted into s.c. tissue, developed lobular carcinoma in situ was observed (**Figure 3D**). It should be noted that the allograft model of miPS-BT549cmP1 tumor the Bdm tumor specimen was transplanted into s.c. tissue (miPS-BT549cmP1MFP/sc) resembled ADH and ILC, while the Bds.c. tumor transplanted from s.c. tissue to s.c. tissue (miPS-BT549cmP1sc/sc) showed infiltrated ductal carcinoma like structures (**Figure 3E**, **3F**).

Tumors obtained from mice transplanted with miPSCs on one side of the 4G of the MFPs showed different germ layers of a teratoma, such as skin and hair (ectoderm in origin), consisting of keratinized stratified squamous epithelium (**Figure 3G**), while tumors obtained

found (**Figure 2C**, **2D**). Adenosis was observed only in mouse Ts.c. tumors from miPS-T47Dcm cells transplanted into s.c. tissue (**Figure 2E**). These results were compared with those from tumors developed from tumor tissue specimens. The Tdm tumor of miPS-T47DcmP1 was directly transplanted into s.c. tissue (miPS-T47DcmP1MFP/sc) showed DCIS as well as ILC like structures (**Figure 2F**), while active mito-
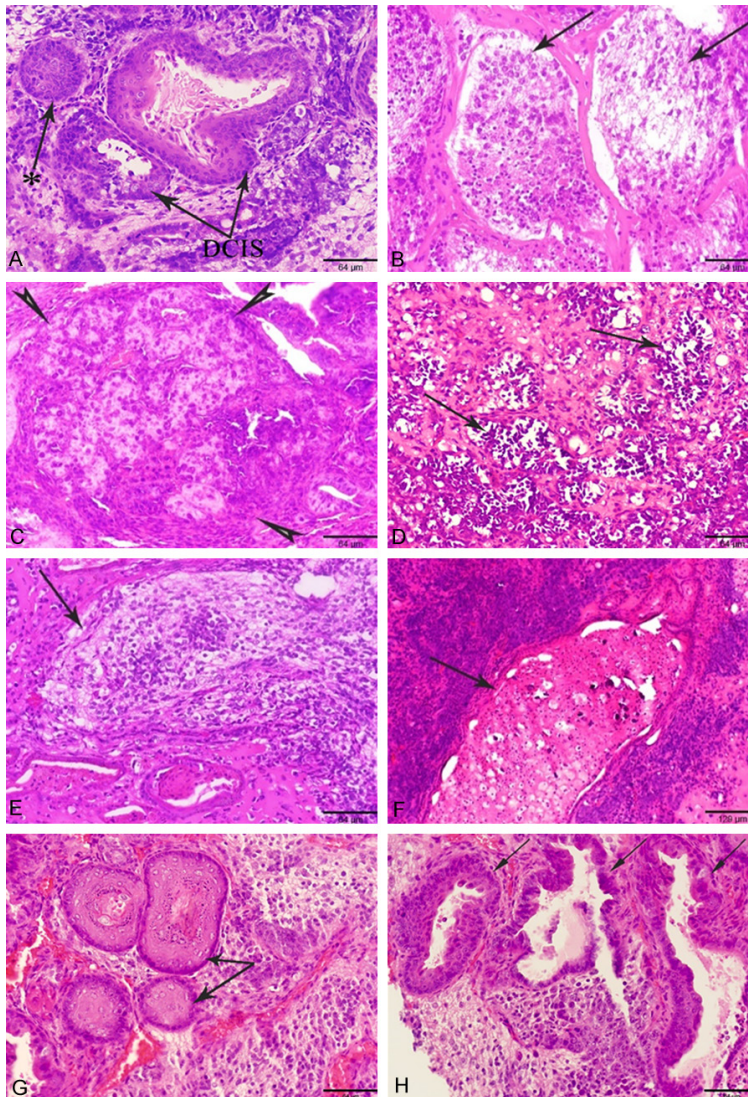
Figure 3. Histopathological observations in the sections of tumors, Bm1, Bm2, Bm3, Bs.c., Bdm and Bds.c. were developed from miPS-BT549cm cells transplanted in BALB/c-nu/nu mice and benign teratoma developed from miPSCs. (A-C, E, G) Tumors developed in MFP (D, F, H) Tumors developed in s.c. Arrows indicate high grade DCIS with comedo necrosis and solid DCIS* with completely filled duct with enlarged and pleomorphic nuclei (A), ILC (B), medullary carcinoma (C), lobular carcinoma in situ (D), ILC (E), infiltrated ductal carcinoma (F), hair follicles (G), and gastrointestinal structures (H) like structures, Hematoxylin and Eosin, scale bar = 129 µm at 10× magnification, 64 µm at 20× magnification.

miPS-BT549cm cells exhibited more malignancy and aggressiveness when transplanted into the MFPs than into s.c. tissue. However, miPS-T47Dcm cells did not exhibit BC characteristics when transplanted into s.c. tissue as the primary and secondary generations of Ts.c./Bs.c. and Tds.c./Bds.c tumors. Even Tm3 tumors, which were the tertiary generation of cells transplanted into the MFPs, lost BC characteristics and exhibited metastasis into lymph nodes, which are often observed in malignant BC. Hence, we focused on the primary tumors, Tm1/Bm1, transplanted into the MFPs, in the following analyses to evaluate the differences between MFP- and s.c.-microenvironments comparing the MFP tumors with tumors transplanted into s.c. tissue, Ts.c/Bs.c. and Tdm/Bdm, so that the effect of MFP microenvironment could be distinguished from that of s.c. microenvironment.

Markers in the tumors correlated with the microenvironment

To address the presence of hormone receptors in the models, immunostaining was performed in Tm1/Bm1, Ts.c./Bs.c. and Tdm/Bdm tumors. The immunoreactivity to ERα/β, PR, PRL-R, Ki67, CK8 and CD44 was evaluated (**Figures 4**, **5**). Immunoreactive ERβ was detected in Tm1/Bm1 tumors transplanted into the MFPs from both miPS-T47Dcm and miPS-BT549cm cells (**Figure 4**). The Bdm tumor showed strong immunoreactivity for PR (**Figure 5C**), while immunoreactivity was moderate in the Bm1 tumor of miPS-BT549cm cells transplanted into the MFPs, and low immunoreactivity was low in the Ts.c. tumor of miPS-T47Dcm cells transplanted into s.c. tissue (**Figure 4B**). On the other hand,

from mice in which miPSCs were transplanted into s.c. tissue showed gastrointestinal structures (endoderm in origin) lined with simple columnar epithelium in the intestine as well as nonkeratinized stratified squamous epithelium identical to those in the esophagus (**Figure 3H**).

The characteristics of all the tumors are summarized in **Table 2**. Both miPS-T47Dcm and
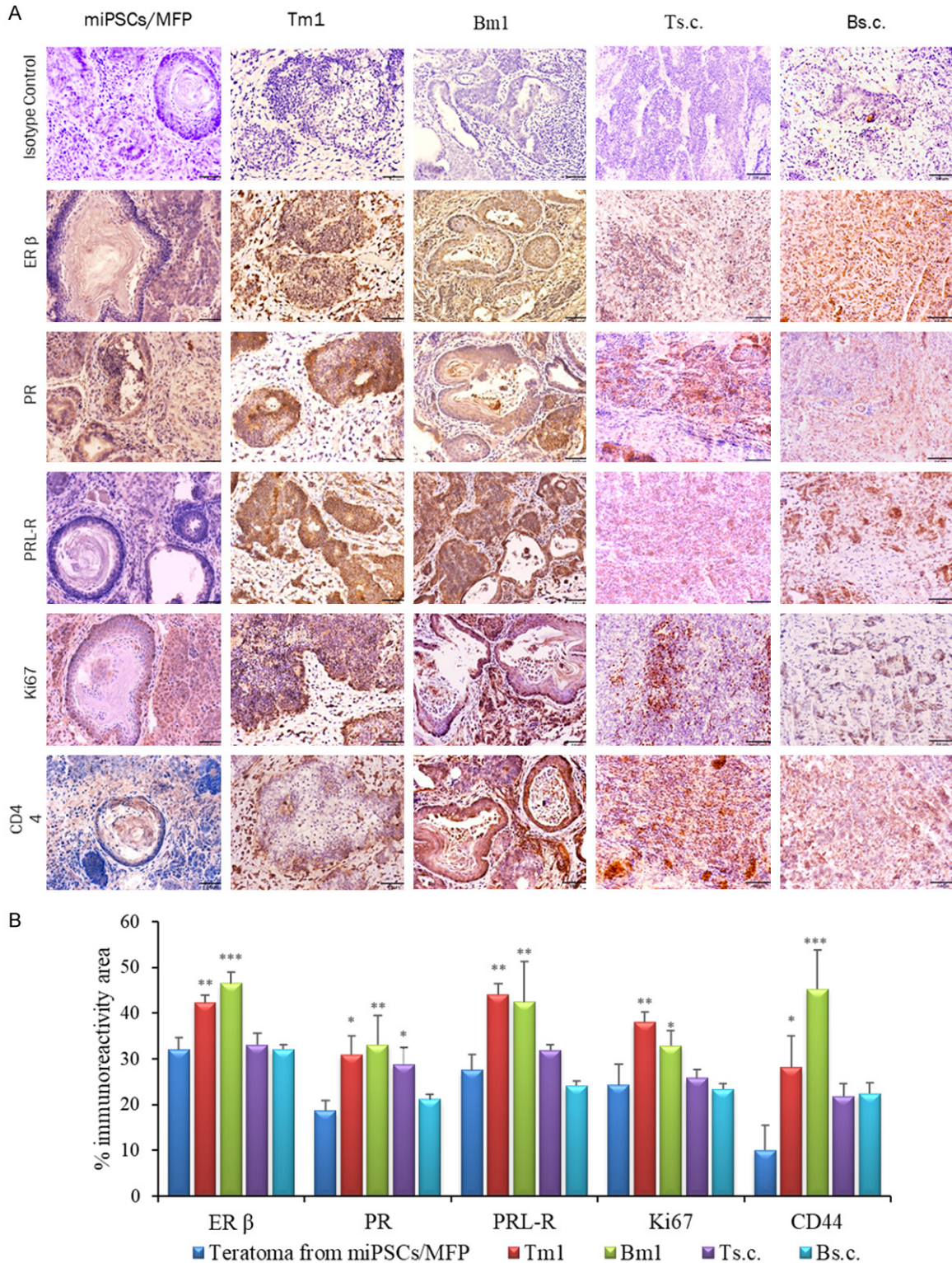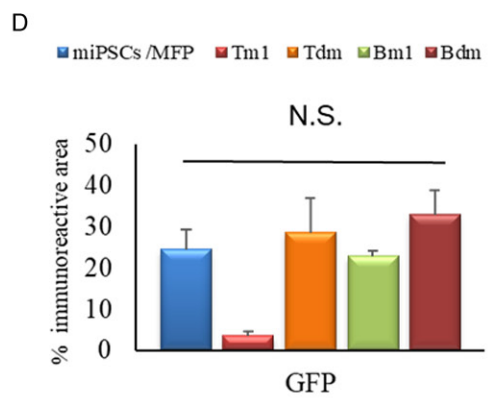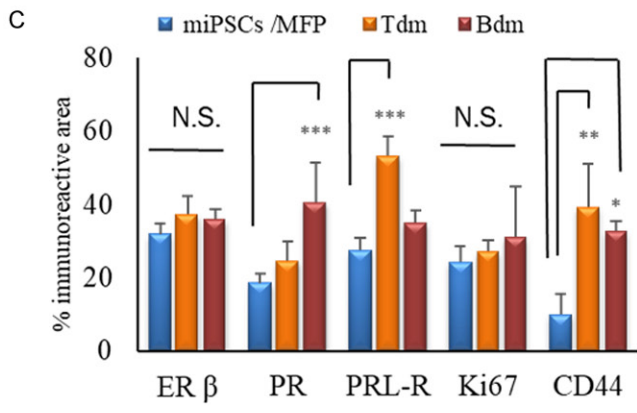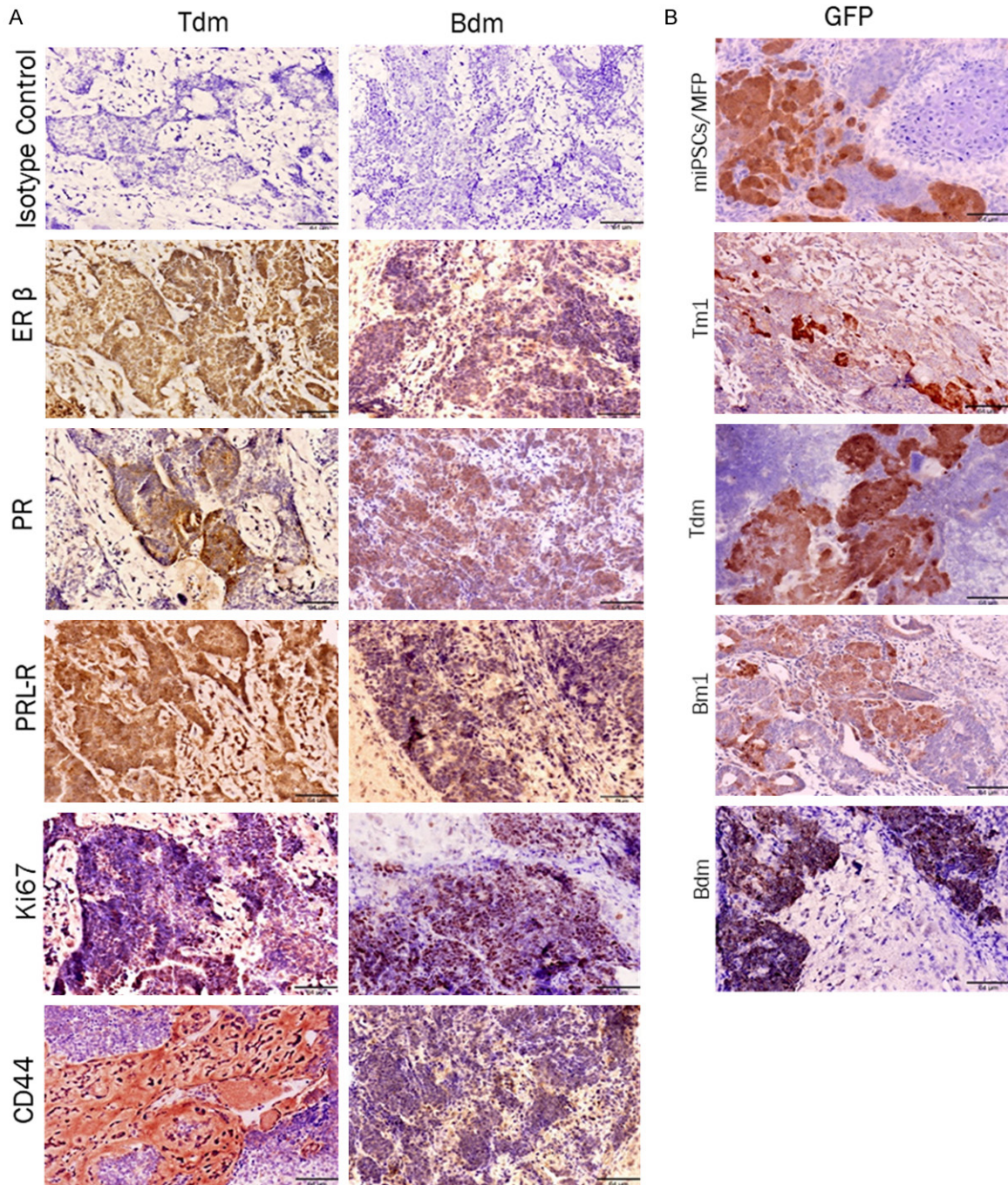
Figure 4. IHC analysis of primary Tm1/Bm1 and Ts.c./Bs.c. tumors transplanted into the MFPs and s.c. tissue, respectively. A. Immunoreactivity to ERβ, PR, PRL-R, Ki67 and CD44 is shown in paraffin sections of Tm/Bm1 and Ts.c./Bs.c. tumors derived from miPS-T47Dcm and miPS-BT549cm cells. Scale bar = 64 µm at 20× magnification. B. Percentage of the immunoreactive area (mean ± SD) of ERβ, PR, PRL-R, Ki67 and CD44 in the different experimental groups. Each bar in the graphs represents the average of six readings (mean ± SD). Significance compared with tumors derived from miPSCs transplanted into the MFPs. *P<0.05, **P<0.01, ***P<0.001.

Mammary fat pad affected CSC derived tumors

Figure 5. IHC analysis of Tm1/Bm1 and Tdm/Bdm tumors sections transplanted into MFP and s.c. tissue, respectively. A. Immunoreactivity to ERβ, PR, PRL-R, Ki67 and CD44 is shown in paraffin sections of Tdm/Bdm, both derived from Tm1 and Bm1 tumors transplanted into s.c. tissue. B. The immunoreactivity of GFP in all Tm1/Bm1, Tdm/Bdm and miPSCs tumor in MFP. Scale bar = 64 µm at 20× magnification. C, D. Percentage of the immunoreactive area (mean ± SD) of ERβ, PR, PRL-R, Ki67, CD44 and GFP expression in the different experimental groups. Each bar in the graphs represents the average of six reading (mean ± SD). Significant compared with tumors derived from miPSCs transplanted into the MFPs. *P<0.05, **P<0.01, ***P<0.001.

PRL-R was strongly detected in the membranes and cytoplasm of all ducts in the Tdm tumor (**Figure 5C**). Simultaneously, moderate immunoreactivity for PRL-R was found in the Tm1/Bm1 tumors of both miPS-T47Dcm and miPS-BT549cm cells transplanted into the MFPs, while strong immunoreactivity for CD44 was observed in the Bm1 and Tdm tumors (**Figure 4B**). The immunoreactivity for GFP was relatively weak overall (**Figure 5B**, **5D**). The proliferation marker Ki67 was recognized as moderately immunoreactive in the Tm1 tumor of miPS-T47Dcm cells transplanted into the MFPs (**Figure 4B**). The immunoreactivities for the markers in the tumors (**Figures 4B**, **5C**) are summarized in **Table 3**. In summary, Tm1/Bm1, Ts.c./Bs.c. and Tdm/Bdm tumors exhibited comparably strong immunoreactivity for ERβ, while Ts.c./Bs.c. tumors exhibited comparably weaker immunoreactivity for PR, PRL-R, Ki67 and CD44 than Tm1/Bm1 and Tdm/Bdm tumors. The MFP, as the tumor microenvironment, appears more effective in exerting mammary tumor-like features than s.c. tissue. Considering the results obtained from Tdm/Bdm tumors, these features appeared to be fixed in the primary tumors and sustained in the secondary tumors even when the microenvironment was changed to s.c. tissue.

Immunofluorescent staining of ERα and CK8 in the Tm1/Bm1 and Ts.c./Bs.c. tumors was assessed (**Figure 6**). The immunoreactivity for ERα was detected in the cytoplasm and membrane in different sections of the Tm1/Bm1, Ts.c./Bs.c., Tdm/Bdm tumors (**Figures 6A** and **7A**), while it was negative in the teratoma derived from miPSCs transplanted into the MFPs (**Figure 6A**). The merged pattern of ERα and GFP was yellow, indicating that ERα was localized in the cytoplasm in the Tm1 tumor of miPS-T47Dcm cells. Immunoreactivity for CK8 was detected in each tumor allograft model (**Figures 6B** and **7B**). However, the colocalization of CK8 and GFP was evident in the Bm1 tumor of miPs-BT549cm cells transplanted into the MFPs, exhibiting a yellow pattern when

merged (**Figure 6B**). The immunoreactivity for GFP and cytoplasmic localization were confirmed at the same time as the reference undifferentiated marker.

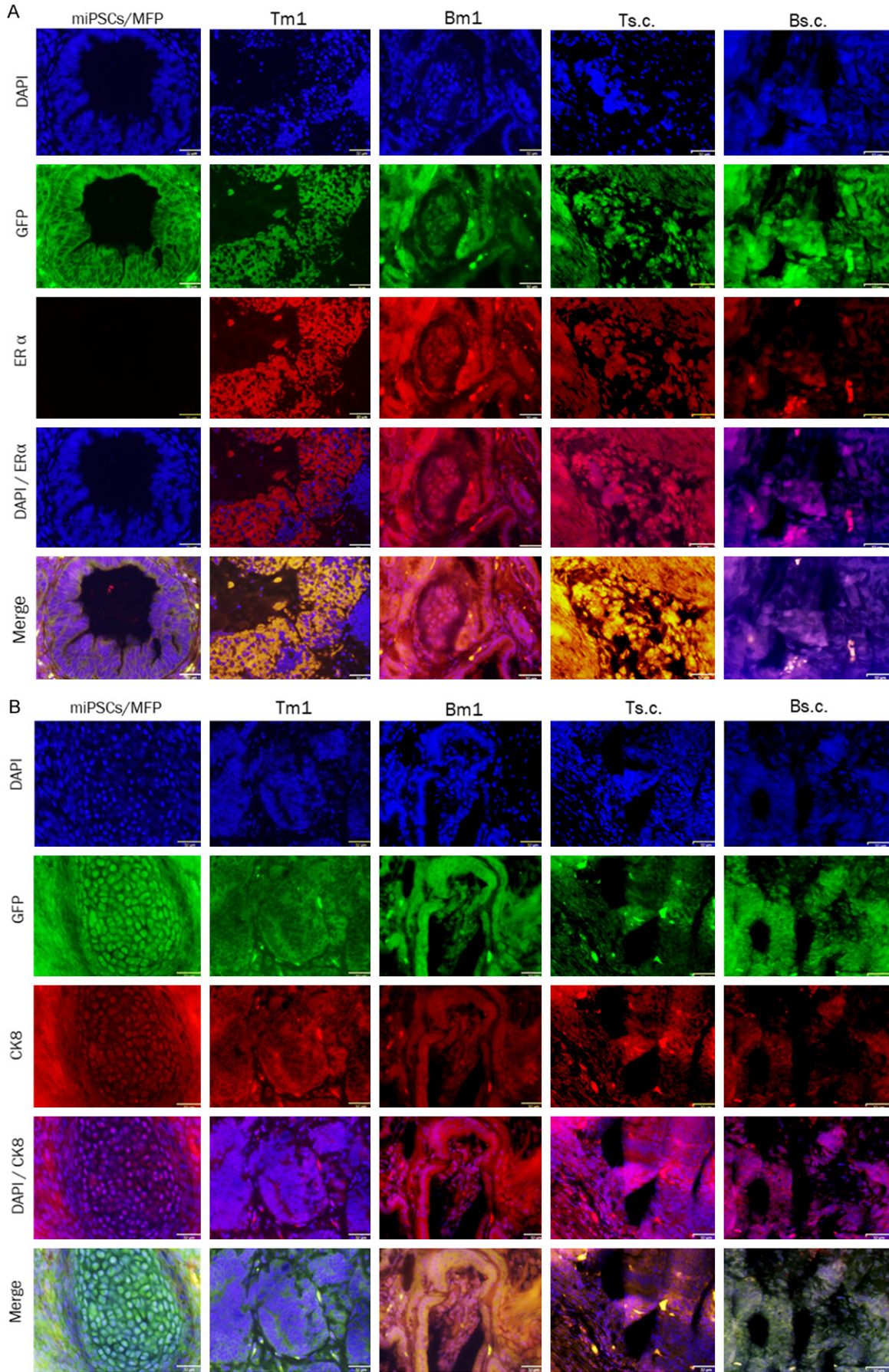*Markers in primary cells correlated with the tumor microenvironment*

Subsequently, we assessed the immunoreactivity for ERα and PR in the primary cells from Tm1/Bm1 and Ts.c./Bs.c. tumors (**Figures 8** and **9**). Both ERα and PR were observed in the nuclei and cytoplasm of miPS-T47Dcm, miPS-BT549cm, miPS-T47DcmP1MFP, miPS-T47DcmP1sc, miPS-BT549cmP1MFP and miPS-BT-549cmP1sc whereas T47D cells were put for the reference of immunoreactivity. The miPS-T47DcmP1MFP cells appeared more differentiated (reddish in color), while miPS-T47DcmP1sc cells appeared undifferentiated (yellowish in color) when GFP and ERα were merged. Based on the immunoreactivity for ERα, miPS-BT549cmP1MFP cells appeared more undifferentiated than miPS-BT549cm P1sc cells when GFP and ERα were merged.

Based on the immunoreactivity for PR, the localization of PR and cell differentiation were not very different between miPS-T47DcmP1MFP cells and miPS-T47DcmP1sc cells. On the other hand, miPS-BT549cmP1MFP cells appeared to be more differentiated (reddish in color), while miPS-BT549cmP1sc cells appeared to be undifferentiated (green in color) when GFP and ERα were merged. PR was localized to the nuclei in both miPS-BT549cmP1MFP cells and miPS-BT549cmP1sc cells, where its immunoreactivity was recognized. In summary, the MFP appears to be a more effective microenvironment to evoke the differentiated mammary phenotype than s.c. tissue.

Markers in the tumors correlated with BC

We further assessed the expression of ERα, ERβ and CK8 using Western blotting (**Figure 10A**, **10B**). The expression of ERα, ERβ and

Figure 6. Immunofluorescence analysis of primary Tm1/Bm1 tumors transplanted into the MFPs and Ts.c./Bs.c. tumors transplanted into s.c. tissue. Immunoreactivity to both ERα and CK8 was detected in paraffin sections from Tm1/Bm1 and Ts.c./Bs.c. tumors derived from miPS-T47Dcm and miPS-BT549cm cells. A. ERα immunoreactivity (red) was observed in the cytoplasm and membrane of tumor cells. B. CK8 immunoreactivity (red) was detected in the cytoplasm and perinucleus of tumor cells. Scale bar = 32 μm at 40× magnification.
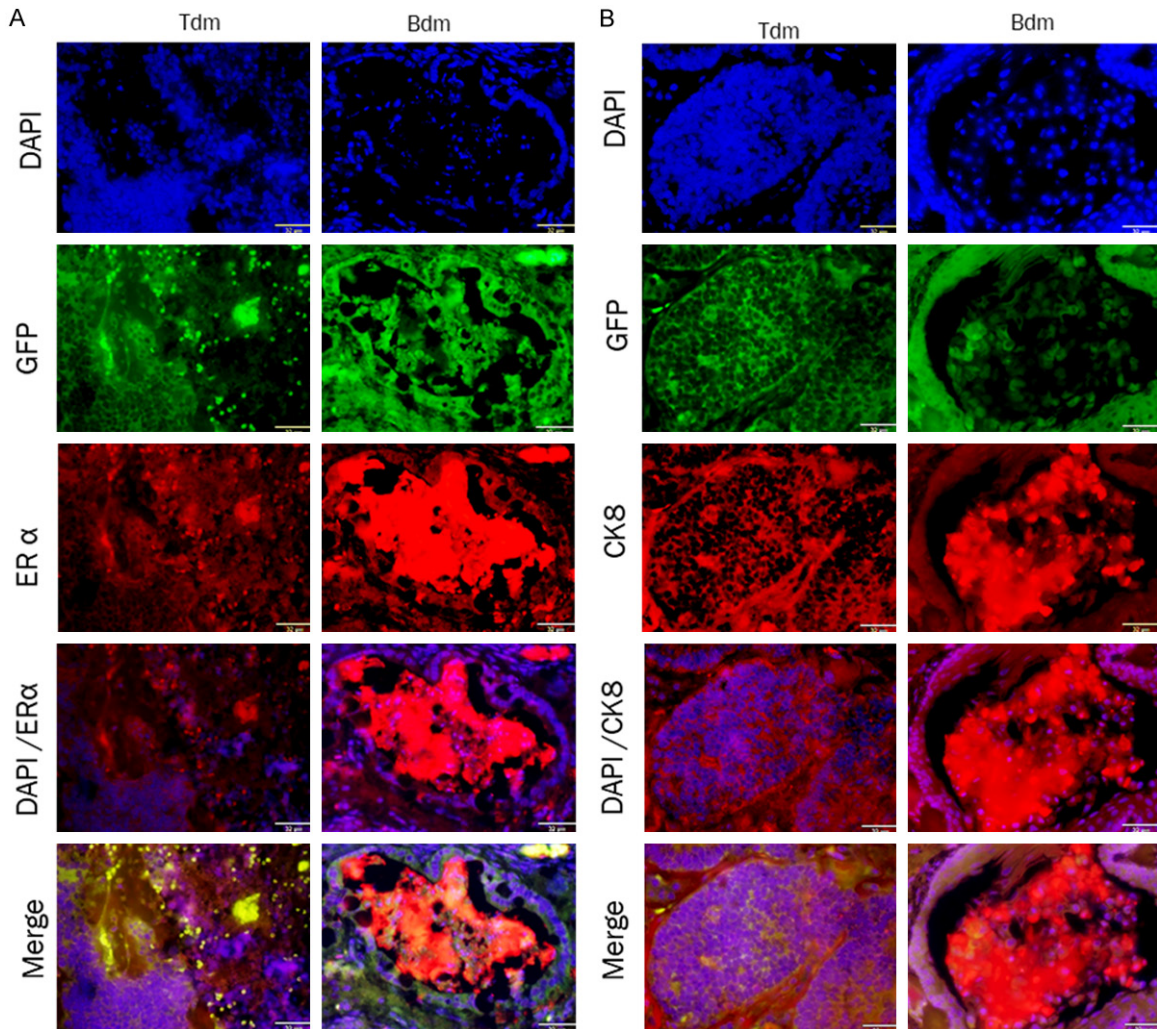

Figure 7. Immunofluorescence analysis of paraffin sections from Tdm and Bdm tumors. The immunoreactivity of both ERα and CK8 were detected in theses sections that derived from Tm1 and Bm1 tumors transplanted into s.c. tissue. A. ERα immunoreactivity (red) was observed in the cytoplasm and membrane of the tumor sections. B. CK8 immunoreactivity (red) was detected in the cytoplasm and perinuclear of tumor sections. Scale bar = 32 μm at 40× magnification.

CK8 was approximately 3- to 5-fold higher in the Tm1 and Ts.c. tumors of miPS-T47Dcm cells transplanted into the MFPs and s.c. tissue than those of NMuMG cells, while the expression of ERβ was approximately 3.8- and 4-fold higher only in the Bm1 and Bs.c. tumors of miPS-BT549cm cells transplanted into the MFPs and s.c. tissue than those of NMuMG cells, respectively. However, in the Tds.c./Bds.c. and Tdm/

Bdm tumors, where mitogenic figures and invasion were observed (**Figure 10B**), the expression of CK8 as well as ERα and ERβ was significant (**Figure 10C**). CK8 immunoreactivity was high in the Ts.c. and Tm1 tumors of miPS-T47Dcm cells due to the presence of invasive mitogenic cells and ILC while its immunoreactivity was only slight in the Bs.c. and Bm1 tumors of miPS-BT549cm cells because no
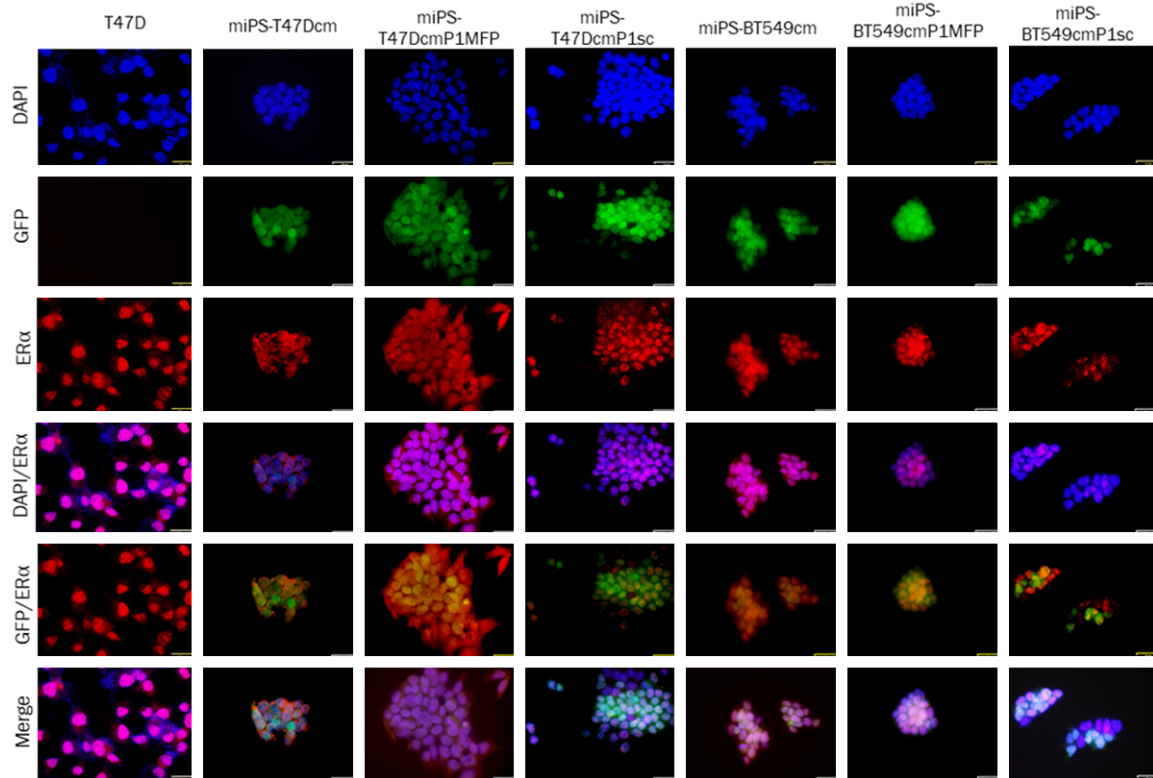
Figure 8. Immunocytochemical analysis of ERα in T47D, miPS-T47Dcm, miPS-T47DcmP1MFP miPS-T47DcmP1sc, miPS-BT549cm, miPS-BT549cmP1MFP and miPS-BT549cmP1sc cells. ERα immunoreactivity (red) was detected in the nuclei, cytoplasm and membrane of different cells. Scale bar = 32 μm at 40× magnification.

invasion was detected in these tumors. From these results, *in vivo* transplantation into either the MFPs or s.c. tissue appear to enhance the characteristics of BC. However, treatment with the CM of T47D cells was more effective than those of BT549 cells in inducing BC characteristics.

Stemness markers in developed tumors

The expression of the stemness markers NANOG, SOX2, KLF4 and OCT3/4 was assessed in the Ts.c./Bs.c., Tm1/Bm1 and Tdm/Bdm tumors by RT-PCR (**Figure 11**). In the Ts.c. and Tm1 tumors of miPS-T47Dcm cells, the stemness markers were highly expressed. The expression of NANOG was enhanced in both miPS-T47Dcm and miPs-BT549cm cells. The expression of KLF4 was distinguished in the Tm1 tumor of miPS-T47Dcm cells, while it was suppressed in miPS-T47Dcm cells, miPS-BT549cm cells, the Ts.c. tumor of miPS-T47Dcm cells, and the Bm1 tumor of miPS-BT549cm cells. Alternatively, the expression of SOX2 was enhanced in both Ts.c./Bs.c tumors. The

expression of OCT3/4 was detected in all tumors and cells. These results indicated that the Ts.c./Bs.c. and Tm1/Bm1 tumors of both miPS-T47Dcm and miPS-BT549cm cells contained undifferentiated cells.

Discussion

BC is typically heterogeneous, probably due to the presence of undifferentiated cancer cells with stemness (so-called CSCs), which exhibit variously differentiated phenotypes depending on the microenvironment. In this study, we evaluated the phenotypes of CSCs that were previously prepared from miPSCs by treatment with the CM of the human breast cancer cell lines T47D and BT549. These two different subtypes of breast carcinoma-derived cells were selected to evaluate the potential to confer the different characteristics of breast carcinomas to CSCs.

The histopathological characteristics of the tumors transplanted into the MFPs were compared to those transplanted into s.c. tissue.
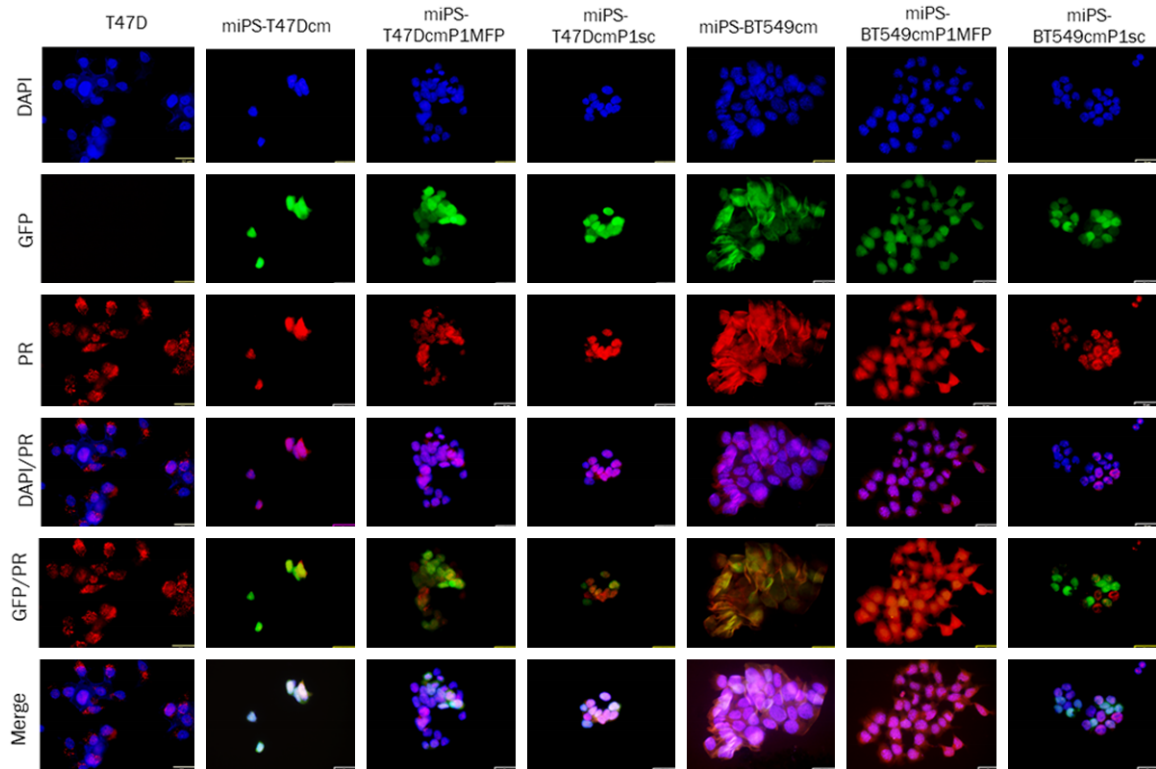
Figure 9. Immunocytochemistry analysis of PR in T47D, miPS-T47Dcm, miPS-T47DcmP1MFP, miPS-T47DcmP1sc, miPS-BT549cm, miPS-BT549cmP1MFP and miPS-BT549cmP1sc cells. PR immunoreactivity (red) was detected in the nuclei and cytoplasm of different cells. Scale bar = 32 μm at 40× magnification.

Two different CSC models of miPS-T47Dcm and miPS-BT549cm cells provided different subtypes of tumors, including DCIS, invasive ductal carcinoma (IDC) and ILC, depending on the site of transplantation, while BC can be categorized into more than 21 different histological types based on the architecture, morphology and growth patterns of cells [20]. ILC is the second most common type of BC after IDC, representing the most aggressive pathological phenotype [21-23]. ILC is observed in the range of approximately 10 to 15% of all types of breast cancer. The presence of ILC makes the diagnosis significantly more precise [24]. In some reports, the diagnosis of ILC was characterized by a large tumor size and positive expression of both ER and PR [25-29]. This agrees with our observation of ILC in this study. The tumors in the first to third stages of miPS-BT549cm cells showed high aggressiveness when transplanted into either the MFPs or s.c. tissue. This aggressiveness is much higher than that of miPS-T47Dcm cells. Although miPS-BT549cm cells exhibited aggressiveness similar to triple-negative breast carcinoma, miPS-BT549cm

CSCs are not derived from triple-negative carcinoma. This result indicated that CM derived from BT549 cells, which are derived from a triple-negative subtype, was not the critical determinant that induced the identical features of cancers in miPSCs affected by CM. Although the effect of the microenvironment on cancer initiation should be investigated further at this point, our results suggest that the MFPs may allow the TME to serve as a platform of tumor growth, as summarized in **Table 2**. Both miPS-T47Dcm and BT549cm cells developed malignant and aggressive tumors when transplanted into the MFPs, while miPS-T47Dcm cells did not develop malignant and aggressive tumors when transplanted into s.c. tissue. This means that the malignancy of tumors depends not only on the characteristics of CSCs but also on the TME.

The crucial role of the MFPs in the development of tumors has been described in different studies following the transplantation of carcinoma-derived cells into the MFPs. The tumor cells transplanted into the 4G of MFPs exhibited dis-
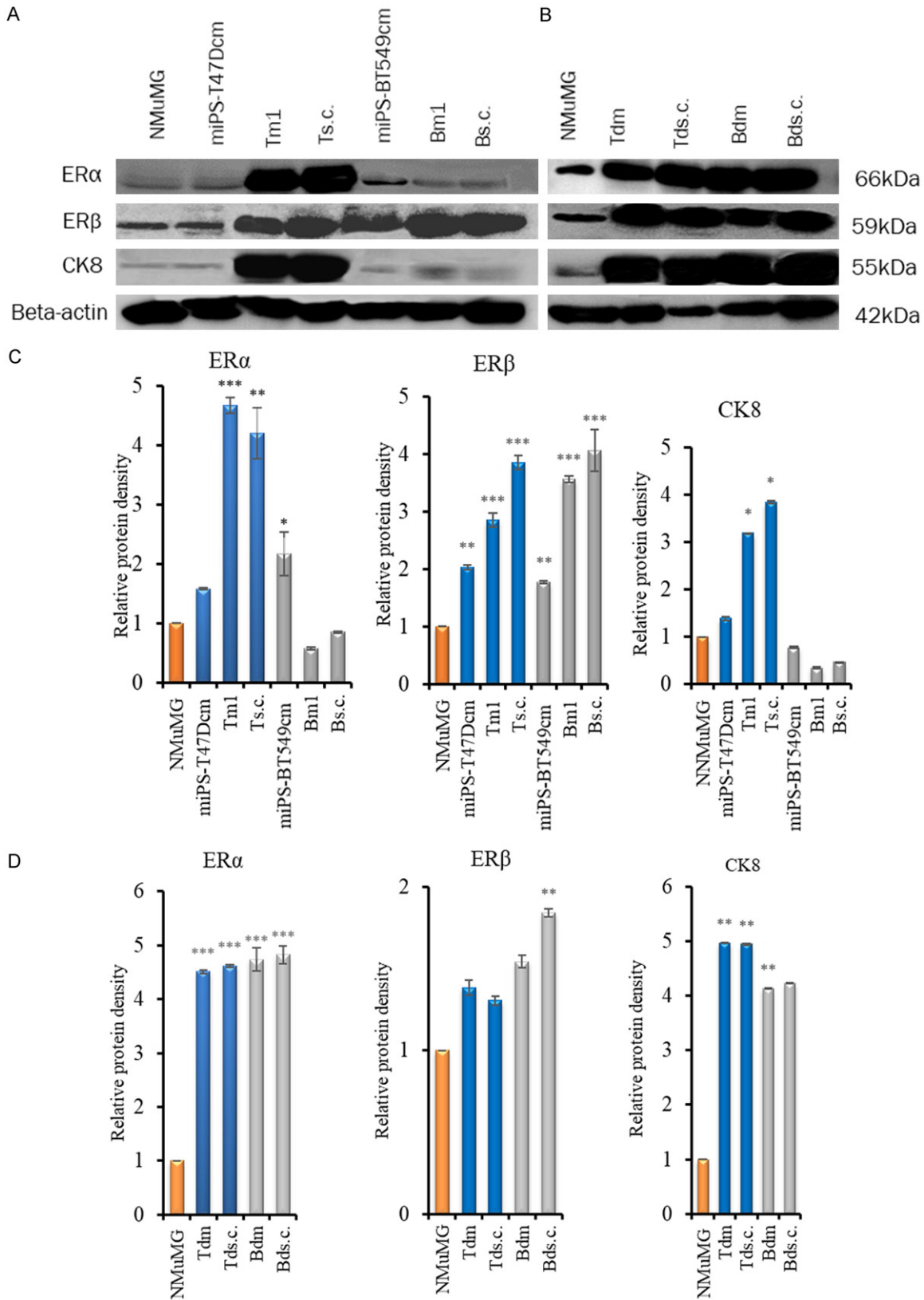
Figure 10. Immunoreactive BC markers in different types of cells and tissues. A, B. Western blot analysis of ERα, ERβ and CK8. C, D. Densitometric analysis of the western blots with ImageJ. C. NMuMG cells, miPS-T47Dcm cells, Tm1 and Ts.c. tumors of miPS-T47Dcm cell transplants, miPS-BT549cm cells, and Bm1 and Bs.c. tumors of miPS-

BT549cm cell transplants (from left to right). D. NMuMG cells, Tdm, Tds.c., Bdm and Bds.c. tumors from miPS-T47DcmP1MFP, miPS-T47DcmP1sc, miPS-BT549cmP1MFP and miPS-BT549cmP1sc tumors (from left to right). The density of each band was normalized to that of β-actin. Each bar in the graphs represents the average of three readings (mean ± SD). *$P<0.05$, **$P<0.01$, ***$P<0.001$.
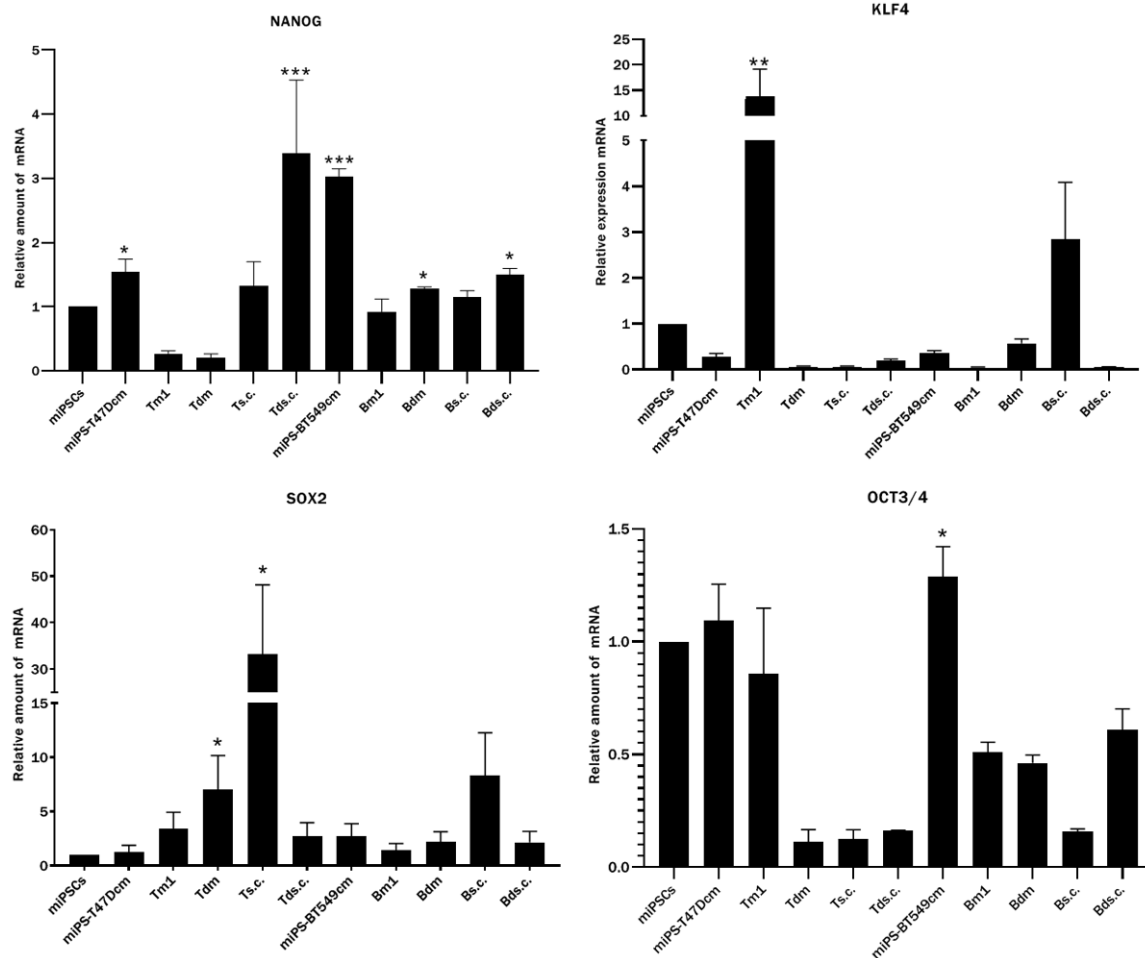

Figure 11. The expression of stemness markers analyzed by RT-qPCR. Expression of stemness markers NANOG, KLF4, SOX2 and OCT3/4 in miPSCs, miPS-T47Dcm cells, tumors Tm1, Tdm, Ts.c., Tds.c. of miPS-T47Dcm cell transplants, miPS-BT549cm cells, tumors Bm1, Bdm, Bs.c., Bds.c. of miPS-BT549cm cell transplants (from left to right). Each bar in the graphs represents the average of three reactions (mean ± SD). The significance was compared with the expression in miPSCs. *$P<0.05$, **$P<0.01$, ***$P<0.001$.

tinguished growth from those transplanted into other sites, such as the perirenal region, meso-metrium, and s.c. tissue [30]. Another study demonstrated the extensive growth of tumors when breast cancer-derived adenocarcinoma cells were coinjected with adipose tissue from mice into the MFPs and s.c. tissue. Since this growth was clearly distinguished from that of the xenografts of cells without adipocytes, the role of adipose tissues from the MFPs was found to be significantly important for encouraging tumor growth [31]. Adipocytes are one of the stromal cells rich in breast tissue that affect the growth of CSCs by secreting various cytokines, chemokines, growth factors and other factors [32-34]. The effects of the microenvironment of the MFPs on growth kinetics, tumor histology and drugs have recently been compared to those of patient-derived xenografts in mice [35]. The tumors in all tested cases were found to be more significantly affected in the MFPs than in s.c. tissue. Considering that the adipose tissue of the MFPs is enriched with saturated fatty acids and mono- and polyun-
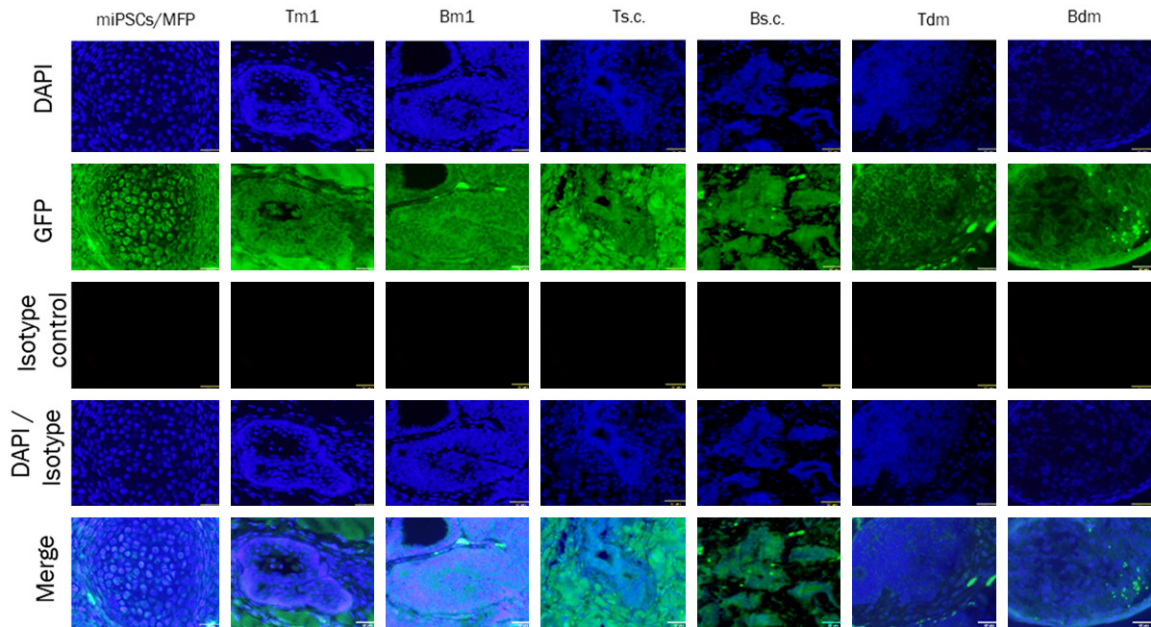
Figure 12. Immunofluorescence analysis of isotype control in different groups by using primary isotype mouse IgG antibody. The immunoreactivity of isotype control was detected in paraffin sections of tumors miPSCs/MFP, Tm1, Bm1, Ts.c., Bs.c., Tdm and Bdm. Scale bar = 32 μm at 40× magnification.

Table 1. Sequences of primers used in the study

Gene name	Accession No.	Forward Primer 5'→3'	Reverse Primer 5'→3'
GAPDH	NM_008084	AACGGCACAGTCAAGGCCGA	ACCCTTTTGGCTCCACCCTT
NANOG	NM_028016.3	AGGGTCTGCTACTGAGATGCTCTG	CAACCACTGGTTTTTCTGCCACCG
KLF4	NM_010637.3	GCGAACTCACACAGGCGAGAAACC	TTATCGTCGACCACTGTGCTGCTG
SOX2	NM_011443.4	TTGCCTTAAACAAGACCACGAAA	TTGCCTTAAACAAGACCACGAAA
OCT3/4	NM_013633.3	TCTTTCCACCAGGCCCCCGGCTC	TGCGGGCGGACATGGGGAGATCC

saturated fatty acids are depleted, probably due to lipolytic agents, the oxidative metabolism of estrogen could enhance the hydroxylation of estrone to hydroxylated forms [36]. The release of fatty acids from adipocytes of the MFPs is altered by the presence of the epithelium [37]. In this context, the coexistence of the MFPs and tumor-derived epithelium can have a characteristic influence on tumor growth [38].

The obtained phenotypes of miPSC-derived CSCs were characterized by mammary tumor-related markers such as ERα/β, PR, PRL-R and CK8 together with common carcinoma markers such as Ki67 and CD44 and stemness markers such as NANOG, SOX2, OCT3/4 and KLF4. These features are rather characteristic of the Tm1/Bm1 tumors from both miPS-T47Dcm and miPS-BT549cm cells, indicating the supporting effects of the MFPs (**Table 3**). One of the impor-

tant features in the growth of BC can be explained by the enhanced expression of cyclin D1 by the binding of ERα to the promoter [39], while the expression of ERβ suppressed by the progression of BC [40]. Nevertheless, many studies have indicated a significant role for ERβ in mammary tumorigenesis [41]. Progesterone reacts with PR within cells in an endocrine manner, which induces the activation of mammary stem cells, which were believed to induce the migration of primary tumor cells [42]. Prolactin stimulates cell proliferation and migration in breast tumorigenesis by binding to PRL-R, which is believed to indicate the risk of BC [43-45]. The expression of CK8 is hypothesized to be related to ILC [46-49]. Collectively, the detected markers in this study could indicate that miPS-T47Dcm and miPS-BT549cm cells are miPSC-derived CSCs.

Table 2. Morphological characteristic of tumors obtained by transplantation

CSCs		miPS-T47Dcm				miPS-BT549cm		
Site	Tumor	BC type	Other type	Malignancy	Tumor	BC type	Other type	Malignancy
MFP	Tm1	ILC	-	+++	Bm1	DCIS, solid DCIS	-	++
	Tm2	ADH, solid DCIS	-	++	Bm2	ILC	-	+++
	Tm3	-	Duct ectasia, fatty necrosis, adenosis, lymph node metastasis	+*	Bm3	Medullary carcinoma	-	++
s.c.	Tdm	DCIS, ILC	-	+++	Bdm	ADH, ILC	-	+++
	Ts.c.	-	Adenosis	-	Bs.c.	Lobular carcinoma in situ	-	++
	Tds.c.	-	Mitogenic cells, necrotic area	+	Bds.c.	Infiltrated ductal carcinoma	-	++

+, moderate; ++, middle; +++, high; +*, moderate with metastasis. Tm1; miPS-T47Dcm MFP, Tm2; miPS-T47DcmP1MFP, Tm3; miPS-T47DcmP2MFP, Tdm; Tm1direct s.c. transplantation, Ts.c.; miPS-T47Dcm s.c., Tds.c.; Ts.c. direct s.c. transplantation, Bm1; miPS-BT549cm MFP, Bm2; miPS-BT549cmP1MFP, Bm3; miPS-BT549cmP2MFP, Bdm; Bm1direct s.c. transplantation, Bs.c.; miPS-BT549cm s.c., Bds.c.; Bs.c. direct s.c. transplantation.

Table 3. The immunoreactivity of hormonal receptors together with Ki67 and CD44 in the primary and secondary tumors

Site	MFP		s.c.		s.c.	
Tumor	Tm1	Bm1	Ts.c.	Bs.c.	Tdm	Bdm
ERβ	3	3	2	2	2	2
PR	2	2	1	1	1	3
PRL-R	3	3	2	1	4	2
Ki-67	2	2	1	1	1	2
CD44	1	3	1	1	2	2

The scores are depicted according to the average percentage of positively stained area in **Figure 3B**. 4, more than or equal to 50%: 3, more than or equal to 40 and less than 50%: 2, more than or equal to 30 and less than 40%: 1, less than 30%. Tm1; miPS-T47Dcm MFP, Bm1; miPS-BT549cm MFP, Ts.c.; miPS-T47Dcm s.c., Bs.c.; miPS-BT549cm s.c., Tdm; Tm1direct s.c. transplantation, Bdm; Bm1direct s.c. transplantation.

CD44 is a marker of CSCs, and its expression is often high in stem cells associated with CSCs that undergo epithelial-to-mesenchymal transition [50]. The immunohistochemical expression of CD44 has been demonstrated to be higher in in situ tumors than in invasive tumors [51], which agrees with our results. Similarly, in our previous study, we detected the expression of the CD44^{+}/CD24^{-low} population in miPS-T47Dcm and miPS-BT549cm cells by flow cytometry, but its expression was higher in primary cells from tumors transplanted into s.c. tissue [12]. This finding may be related to the enhanced expression of CD44 in miPS-BT549cm cells in the Bm1 tumor, indicating the effect of the MFPs integrated with the characteristics of the CSCs themselves. Moreover, activated CAFs also enhance the expression of stemness markers such as CD44, OCT3/4, NANOG and KLF4 in CSCs [52], agreeing with our observation in miPSC-derived CSCs (**Figure 11**).

In conclusion, we demonstrated that CSCs converted from normal miPSCs under the microenvironment of BC provided different malignant tumorigenic subtypes of BC. The microenvironment of the MFPs was simultaneously shown to be more effective than that of s.c. tissue to develop the subtypes related with BC. In summary, we successfully established a breast cancer tumor model using mouse induced pluripotent stem cells developed from normal fibroblasts without genetic manipulation.

Disclosure of conflict of interest

None.

Abbreviations

BC, Breast cancer; ADH, Atypical ductal hyperplasia; DCIS, Ductal carcinoma in situ; CSCs, Cancer stem cells; iPSCs, Induced pluripotent stem cells; CM, Conditioned medium; CAFs, Cancer-associated fibroblasts; TAMs, Tumor-associated macrophages; TME, Tumor microenvironment; miPSCs, Mouse induced pluripotent stem cells; MFP, Mammary fat pad; s.c., Subcutaneous; FBS, Fetal bovine serum; P/S, Penicillin/streptomycin; MEF, Mouse embryonic fibroblast; 4G, Fourth pair; P, Primary; IHC, Immunohistochemistry; Erβ, Estrogen receptor β; PR, Progesterone receptor; PRL-R, Prolactin receptor; GFP, Green florescent protein; PBS, Phosphate-buffered saline; ERα, Estrogen receptor α; CK8, Cytokeratin 8; DAPI, 4,6-Diamidino-2-phenylindole; RT-qPCR, Reverse transcription quantitative polymerase chain reaction; ILC, Invasive lobular carcinoma; IDC, Invasive ductal carcinoma.

Address correspondence to: Masaharu Seno and Xiaoying Fu, Department of Biotechnology and Drug Discovery, Graduate School of Interdisciplinary Science and Engineering in Health Systems, Okayama University, Okayama 700-8530, Japan. Tel: +81-86-251-8216; E-mail: mseno@okayama-u.ac.jp (MS); fuxiaoyingtj@163.com (XYF)

References

[1] Ferlay J, Soerjomataram I, Dikshit R, Eser S, Mathers C, Rebelo M, Parkin DM, Forman D and Bray F. Cancer incidence and mortality worldwide: sources, methods and major patterns in GLOBOCAN 2012. Int J Cancer 2015; 136: E359-386.

[2] Wellings SR and Jensen HM. On the origin and progression of ductal carcinoma in the human breast. J Natl Cancer Inst 1973; 50: 1111-1118.

[3] Al-Hajj M, Wicha MS, Benito-Hernandez A, Morrison SJ and Clarke MF. Prospective identification of tumorigenic breast cancer cells. Proc Natl Acad Sci U S A 2003; 100: 3983-3988.

[4] Clarke MF, Dick JE, Dirks PB, Eaves CJ, Jamieson CH, Jones DL, Visvader J, Weissman IL and Wahl GM. Cancer stem cells--perspectives on current status and future directions: AACR Workshop on cancer stem cells. Cancer Res 2006; 66: 9339-9344.

[5] Jordan CT, Guzman ML and Noble M. Cancer stem cells. N Engl J Med 2006; 355: 1253-1261.

[6] Dalerba P, Cho RW and Clarke MF. Cancer stem cells: models and concepts. Annu Rev Med 2007; 58: 267-284.

[7] Reya T, Morrison SJ, Clarke MF and Weissman IL. Stem cells, cancer, and cancer stem cells. Nature 2001; 414: 105-111.

[8] Clevers H. The cancer stem cell: premises, promises and challenges. Nat Med 2011; 17: 313-319.

[9] Sheridan C, Kishimoto H, Fuchs RK, Mehrotra S, Bhat-Nakshatri P, Turner CH, Goulet R Jr, Badve S and Nakshatri H. CD44+/CD24- breast cancer cells exhibit enhanced invasive properties: an early step necessary for metastasis. Breast Cancer Res 2006; 8: R59.

[10] Wicha MS. Cancer stem cells and metastasis: lethal seeds. Clin Cancer Res 2006; 12: 5606-5607.

[11] Chen L, Kasai T, Li Y, Sugii Y, Jin G, Okada M, Vaidyanath A, Mizutani A, Satoh A, Kudoh T, Hendrix MJ, Salomon DS, Fu L and Seno M. A model of cancer stem cells derived from mouse induced pluripotent stem cells. PLoS One 2012; 7: e33544.

[12] Nair N, Calle AS, Zahra MH, Prieto-Vila M, Oo AKK, Hurley L, Vaidyanath A, Seno A, Masuda J, Iwasaki Y, Tanaka H, Kasai T and Seno M. A cancer stem cell model as the point of origin of cancer-associated fibroblasts in tumor microenvironment. Sci Rep 2017; 7: 6838.

[13] Osman A, Oze M, Afify SM, Hassan G, El-Ghlban S, Nawara HM, Fu X, Zahra MH, Seno A, Winer I, Salomon DS and Seno M. Tumor-associated macrophages derived from cancer stem cells. Acta Histochem 2020; 122: 151628.

[14] Afify SM and Seno M. Conversion of stem cells to cancer stem cells: undercurrent of cancer initiation. Cancers (Basel) 2019; 11: 345.

[15] Prieto-Vila M, Yan T, Calle AS, Nair N, Hurley L, Kasai T, Kakuta H, Masuda J, Murakami H, Mizutani A and Seno M. iPSC-derived cancer stem cells provide a model of tumor vasculature. Am J Cancer Res 2016; 6: 1906-1921.

[16] Calle AS, Nair N, Oo AK, Prieto-Vila M, Koga M, Khayrani AC, Hussein M, Hurley L, Vaidyanath A, Seno A, Iwasaki Y, Calle M, Kasai T and Seno M. A new PDAC mouse model originated from iPSCs-converted pancreatic cancer stem cells (CSCcm). Am J Cancer Res 2016; 6: 2799-2815.

[17] Afify SM, Sanchez Calle A, Hassan G, Kumon K, Nawara HM, Zahra MH, Mansour HM, Khayrani AC, Alam MJ, Du J, Seno A, Iwasaki Y and Seno M. A novel model of liver cancer stem cells developed from induced pluripotent stem cells. Br J Cancer 2020; 122: 1378-1390.

[18] Okita K, Ichisaka T and Yamanaka S. Generation of germline-competent induced pluripotent stem cells. Nature 2007; 448: 313-317.

[19] Schindelin J, Arganda-Carreras I, Frise E, Kaynig V, Longair M, Pietzsch T, Preibisch S, Rueden C, Saalfeld S, Schmid B, Tinevez JY, White DJ, Hartenstein V, Eliceiri K, Tomancak P and Cardona A. Fiji: an open-source platform for biological-image analysis. Nat Methods 2012; 9: 676-682.

[20] Hanby AM, Walker C, Tavassoli FA and Devilee P. Pathology and genetics: tumours of the breast and female genital organs. WHO Classification of Tumours series - volume IV. Breast Cancer Research. Lyon, France: IARC Press; 2004; 6: 133.

[21] Martinez V and Azzopardi JG. Invasive lobular carcinoma of the breast: incidence and variants. Histopathology 1979; 3: 467-488.

[22] Li CI and Daling JR. Changes in breast cancer incidence rates in the United States by histologic subtype and race/ethnicity, 1995 to 2004. Cancer Epidemiol Biomarkers Prev 2007; 16: 2773-2780.

[23] Lakhani SRE IO, Schnitt SJ, Tan PH, van de Vijver MJ. WHO classification of tumours of the breast. New York: WHO Press; 2012.

[24] Biglia N, Mariani L, Sgro L, Mininanni P, Moggio G and Sismondi P. Increased incidence of lobular breast cancer in women treated with hormone replacement therapy: implications for diagnosis, surgical and medical treatment. Endocr Relat Cancer 2007; 14: 549-567.

[25] Sastre-Garau X, Jouve M, Asselain B, Vincent-Salomon A, Beuzeboc P, Dorval T, Durand JC, Fourquet A and Pouillart P. Infiltrating lobular carcinoma of the breast. Clinicopathologic analysis of 975 cases with reference to data on conservative therapy and metastatic patterns. Cancer 1996; 77: 113-120.

[26] Winchester DJ, Chang HR, Graves TA, Menck HR, Bland KI and Winchester DP. A comparative analysis of lobular and ductal carcinoma of the breast: presentation, treatment, and outcomes. J Am Coll Surg 1998; 186: 416-422.

[27] Korhonen T, Huhtala H and Holli K. A comparison of the biological and clinical features of invasive lobular and ductal carcinomas of the breast. Breast Cancer Res Treat 2004; 85: 23-29.

[28] Mhuircheartaigh JN, Curran C, Hennessy E and Kerin MJ. Prospective matched-pair comparison of outcome after treatment for lobular and ductal breast carcinoma. Br J Surg 2008; 95: 827-833.

[29] Chen Z, Yang J, Li S, Lv M, Shen Y, Wang B, Li P, Yi M, Zhao X, Zhang L, Wang L and Yang J. Invasive lobular carcinoma of the breast: a special histological type compared with invasive ductal carcinoma. PLoS One 2017; 12: e0182397.

[30] Hoshino K. Mammary transplantation and its histogenesis in mice. Baltimore: University Park Press; 1980.

[31] Elliott BE, Tam SP, Dexter D and Chen ZQ. Capacity of adipose tissue to promote growth and metastasis of a murine mammary carcinoma: effect of estrogen and progesterone. Int J Cancer 1992; 51: 416-424.

[32] Lin Q, Lee YJ and Yun Z. Differentiation arrest by hypoxia. J Biol Chem 2006; 281: 30678-30683.

[33] Mohyeldin A, Garzon-Muvdi T and Quinones-Hinojosa A. Oxygen in stem cell biology: a critical component of the stem cell niche. Cell Stem Cell 2010; 7: 150-161.

[34] Carcereri de Prati A, Butturini E, Rigo A, Oppici E, Rossin M, Boriero D and Mariotto S. Metastatic breast cancer cells enter into dormant state and express cancer stem cells phenotype under chronic hypoxia. J Cell Biochem 2017; 118: 3237-3248.

[35] Draheim KM, Banzon RR, Tewodros MM, VanBuskirk D, Cheng M. Comparing subcutanous to mammary fat pad implantation on the growth kinetics, histology and drug response of PDX breast cancer models. AACR Annual Meeting, Philadelphia, PA, April 27-28 and June 22-24; Cancer Res 2020; 1672.

[36] Rebuffe-Scrive M, Eldh J, Hafstrom LO and Bjorntorp P. Metabolism of mammary, abdominal, and femoral adipocytes in women before and after menopause. Metabolism 1986; 35: 792-797.

[37] Kidwell WR, Knazek RA, Vonderhaar BK and Losonczy I. Effects of unsaturated fatty acids on the development and proliferation of normal and neoplastic breast epithelium. New York: Raven Press; 1982.

[38] Neville MC, Medina D, Monks J and Hovey RC. The mammary fat pad. J Mammary Gland Biol Neoplasia 1998; 3: 109-116.

[39] Zwijsen RM, Wientjens E, Klompmaker R, van der Sman J, Bernards R and Michalides RJ. CDK-independent activation of estrogen receptor by cyclin D1. Cell 1997; 88: 405-415.

[40] Huang B, Omoto Y, Iwase H, Yamashita H, Toyama T, Coombes RC, Filipovic A, Warner M and Gustafsson JA. Differential expression of estrogen receptor alpha, beta1, and beta2 in lobular and ductal breast cancer. Proc Natl Acad Sci U S A 2014; 111: 1933-1938.

[41] Saha Roy S and Vadlamudi RK. Role of estrogen receptor signaling in breast cancer metastasis. Int J Breast Cancer 2012; 2012: 654698.

[42] Hosseini H, Obradovic MMS, Hoffmann M, Harper KL, Sosa MS, Werner-Klein M, Nanduri LK, Werno C, Ehrl C, Maneck M, Patwary N, Haunschild G, Guzvic M, Reimelt C, Grauvogl M, Eichner N, Weber F, Hartkopf AD, Taran FA, Brucker SY, Fehm T, Rack B, Buchholz S, Spang R, Meister G, Aguirre-Ghiso JA and Klein CA. Early dissemination seeds metastasis in breast cancer. Nature 2016; 540: 552-558.

[43] Maus MV, Reilly SC and Clevenger CV. Prolactin as a chemoattractant for human breast carcinoma. Endocrinology 1999; 140: 5447-5450.

[44] Vonderhaar BK. Prolactin involvement in breast cancer. Endocr Relat Cancer 1999; 6: 389-404.

[45] Clevenger CV, Furth PA, Hankinson SE and Schuler LA. The role of prolactin in mammary carcinoma. Endocr Rev 2003; 24: 1-27.

[46] Fu N, Lindeman GJ and Visvader JE. The mammary stem cell hierarchy. Curr Top Dev Biol 2014; 107: 133-160.

[47] Visvader JE and Stingl J. Mammary stem cells and the differentiation hierarchy: current status and perspectives. Genes Dev 2014; 28: 1143-1158.

[48] Inman JL, Robertson C, Mott JD and Bissell MJ. Mammary gland development: cell fate specification, stem cells and the microenvironment. Development 2015; 142: 1028-1042.

[49] Lloyd-Lewis B, Harris OB, Watson CJ and Davis FM. Mammary stem cells: premise, properties, and perspectives. Trends Cell Biol 2017; 27: 556-567.

[50] Bhat-Nakshatri P, Appaiah H, Ballas C, PickFranke P, Goulet R Jr, Badve S, Srour EF and Nakshatri H. SLUG/SNAI2 and tumor necrosis factor generate breast cells with CD44+/CD24- phenotype. BMC Cancer 2010; 10: 411.

[51] Park SY, Lee HE, Li H, Shipitsin M, Gelman R and Polyak K. Heterogeneity for stem cell-related markers according to tumor subtype and histologic stage in breast cancer. Clin Cancer Res 2010; 16: 876-887.

[52] Al-Khalaf HH, Ghebeh H, Inass R and Aboussekhra A. Senescent breast luminal cells promote carcinogenesis through interleukin-8-dependent activation of stromal fibroblasts. Mol Cell Biol 2019; 39: e00359-18.